Electronic Supplementary Material (ESI) for Energy & Environmental Science

Supporting Information for:

New insights into the electrochemical reduction of carbon dioxide on metallic copper surfaces

Kendra P. Kuhl,[a] Etosha R. Cave,[b] David N. Abram,[c] Thomas F. Jaramillo[c*]

[a]Department of Chemistry, Stanford University, Stanford, CA 94305-5025 USA

[b]Department of Mechanical Engineering, Stanford University, Stanford, CA 94305-5025 USA

[c]Department of Chemical Engineering, Stanford University, Stanford, CA 94305-5025 USA

*Corresponding Author

E-mail: jaramillo@stanford.edu

Telephone: 650-498-6879; Fax: 650-723-9780

IR compensation

Solution resistance causes a voltage drop between the reference electrode and working electrode which follows Ohm's law: V=I*R.[1] This resistance is commonly referred to as uncompensated resistance (R_u), because the potentiostat does not compensate for it under normal conditions. R_u is dependent upon a number of factors, such as electrolyte, temperature, electrode placement, and electrode size. Since R_u may differ between experiments, it must be corrected for in order to generate consistent data. This is particularly important when comparing data between different laboratories where different experimental setups are used or when comparing to theoretical predictions.

In this study, potentiostatic electrochemical impedance spectroscopy (PEIS) was used to determine R_u. The relationship between an AC potential and the resulting AC current defines the impedance.[2] At high frequency, contributions to the impedance from components of the electrochemical circuit other than R_u become negligible. However, there is a limit to how high of frequency can be used before the measured impedance no longer applies to the electrochemical cell. To find the correct frequency in determining R_u, PEIS was performed at frequencies ranging from 1 MHz to 1 Hz at open circuit potential and -2.1 V vs. a Ag/AgCl reference electrode. 10 kHz was chosen as an appropriate frequency to determine R_u, which corresponds to the real impedance measured at this frequency (Figure S1). Subsequent determinations of R_u were performed only at 10 kHz.

The potentiostat's IR compensation function was used to compensate for 85% of R_u. It is not possible for the potentiostat to compensate for 100% of R_u because it gives rise to instability in potentiostat control.[3] To get the most accurate numbers, the final 15% of Ru was mathematically corrected for after the electrochemical data was collected. The adjustment to the voltage was: $V_{100\%\text{ IR corrected vs. RHE}} = V_{85\%\text{ IR corrected vs. RHE}} - 15\% * \text{average } R_u \text{ (Ohms)} * \text{average I (amps)}$. Figure S2 shows that at higher overpotential and current, the value of R_u decreased over the course of the hour long electrolysis. In order to avoid overcompensating for R_u and to maintain potentiostat stability it was necessary to remeasure the value of R_u periodically. A temperature probe placed in the electrolysis cell revealed that at -1.18 V, the most negative potential tested, the temperature of the electrolyte rose by 3° C over the course of the hour and is likely the cause of the decreased resistance. At lower overpotential and current, R_u did not decrease during electrolysis, but the value still fluctuated about a mean. Variation in the

measured value of R_u had a standard deviation of 0.23 Ω consistent with reference[4] and led to some uncertainty in the voltage measurement (Table S2).

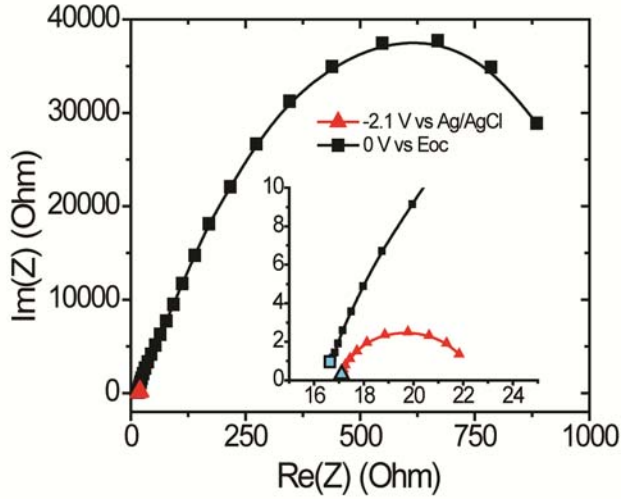

Figure S1. PEIS taken in the electrolysis cell with a Cu working electrode at different potentials. The markers shown in blue indicate the impedance at 10 kHz.

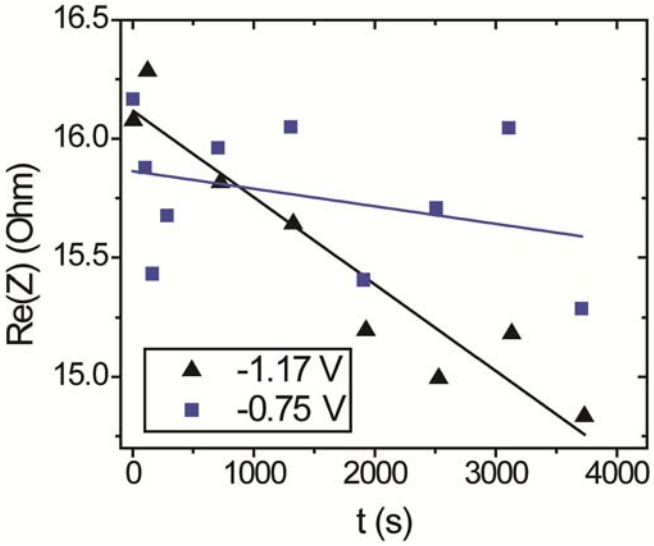

Figure S2. Change in R_u over the course of two electrolysis experiments at different potentials.

Gas chromatography

Briefly, the gas chromatograph, running N_2 as a carrier gas, contained a molecular sieve 13X and a haysep D column which were used together to separate hydrogen, methane, CO, CO_2 and ethylene. After exiting the columns, the gas stream was first analyzed by a thermal conductivity detector (TCD) where hydrogen was detected. The gas stream then passed through

a methanizer where CO and CO_2 were converted to methane for immediate detection by a flame ionization detector (FID) where the carbon containing gas products were quantified. The peak areas for hydrogen, methane, CO, CO_2 and ethylene were compared to standards to find the concentration of each. Figure S3 shows a typical chromatogram with FID and TCD traces.

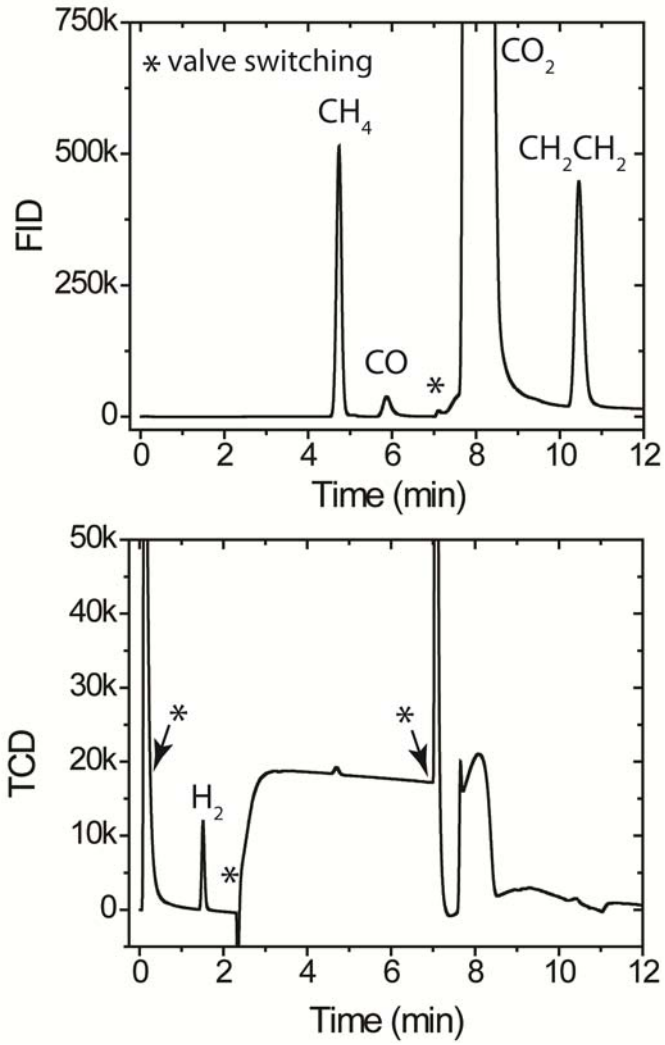

Figure S3. GC traces from FID and TCD channels. Peaks corresponding to the observed gaseous products are indicated.

NMR product quantification

NMR is generally not used quantitatively because differences in the T1s of analytes can lead to differing peak areas when measurements are made under differing conditions, such as different number of scans or solution compositions.[5] In addition, there are other factors, such as shimming and phasing that can cause differences in peak areas. Despite these difficulties, we

found NMR to be extremely useful for detection of electrochemical products because it could be performed directly on the electrolyte solution without the need to remove the $KHCO_3$. To avoid problems arising from the analyte and internal standard having different T1s, the same spectral acquisition parameters were used for all quantification spectra. In addition, solvent suppression was used to decrease the size of the water peak so that the smaller CO_2 reduction product peaks were visible. Figure S4 shows a typical 1D ^1H NMR spectrum collected for quantification on a sample containing commercial standards of CO_2 reduction products and internal standards.

Peak areas of products were compared to internal standards to make standard curves. The internal standards, phenol and DMSO, were chosen because they did not interfere with peaks arising from CO_2 reduction products and because of their non-volatility which allowed for use and storage of the same internal standards solution for all of the product measurements in this study without appreciable change in concentration. The area of product peaks to the right of the water peak was compared to the area of DMSO, and the area of product peaks to the left of the water peak was compared to the area of phenol for preparation of and comparison to standard curves. Figure S5 shows 2-4 standard curves for each product prepared from purchased standards using the peaks indicated in Table S1. Different standard curves for the same product are in good agreement with each other, and when normalized to the number of protons in each of the peaks used to construct the standard curves, the slope of the lines are in good agreement. The linearity of the curves and the agreement of their normalized slopes demonstrate that it was possible in this case to accurately determine the concentration of products in the unknown solutions. Acetaldehyde and propionaldehyde were too volatile to make accurate standard curves, so the average slope/proton found from the normalized standard curves was used. It was also taken into account that the diol and keto forms of acetaldehyde and propionaldehyde are present in a 1:1 ratio in solution when calculating the concentration of each.

The 2D homonuclear COSY was acquired on an 800 MHz Agilent VNMRS (gCOSY pulse sequence) with prescan magnetization randomization, 1 s water presaturation, over an 8000 Hz spectral width (t_1 and t_2) , 256 ms acquisition time, centered on the water peak for 4 scans per 256 t_1 increments.

The 2D ($^1H/^{13}C$) HSQC experiments (data not shown) were acquired on an 800 MHz Varian Inova (gChsqc pulse sequence). An HSQC of the aliphatic carbon region was acquired with 1 s prescan delay, over 14378 Hz/16089 Hz (^1H $t_2/^{13}C$ t_1) spectral widths, ^{13}C decoupling

during 71 ms acquisition time, centered on the water peak (^{1}H t_2) and 35 ppm (^{13}C t_1) for 16 scans per 211 t_1 increments. An HSQC of the aromatic carbon region was acquired with 1 s prescan delay, over 14378 Hz/8045 Hz (^{1}H t_2/^{13}C t_1) spectral widths, ^{13}C decoupling during 71 ms acquisition time, centered on the water peak (^{1}H t_2) and 125 ppm (^{13}C t_1) for 8 scans per 96 t_1 increments. A third HSQC of the downfield carbon region (to identify the downshifted formate H-C) was acquired with 1 s prescan delay, over 14378 Hz/8045 Hz (^{1}H t_2/^{13}C t_1) spectral widths, ^{13}C decoupling during 71 ms acquisition time, centered on the water peak (^{1}H t_2) and 165 ppm (^{13}C t_1) for 8 scans per 96 t_1 increments.

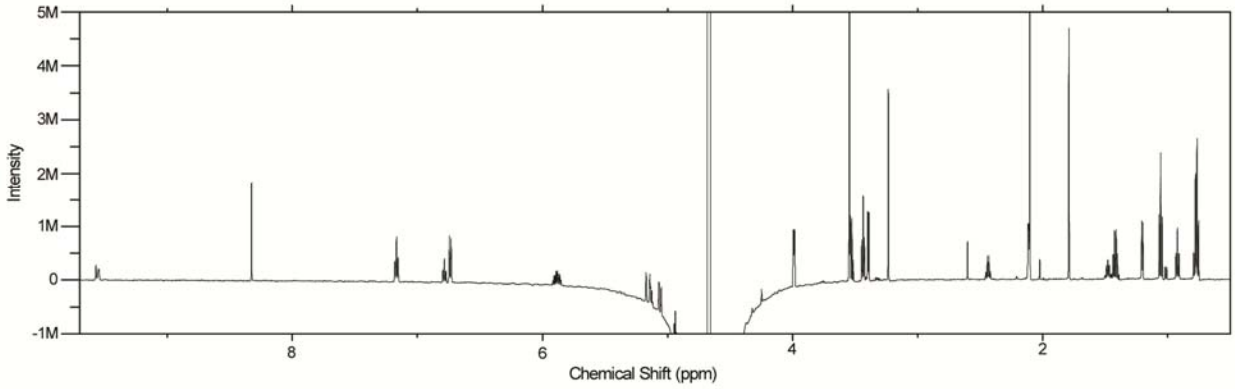

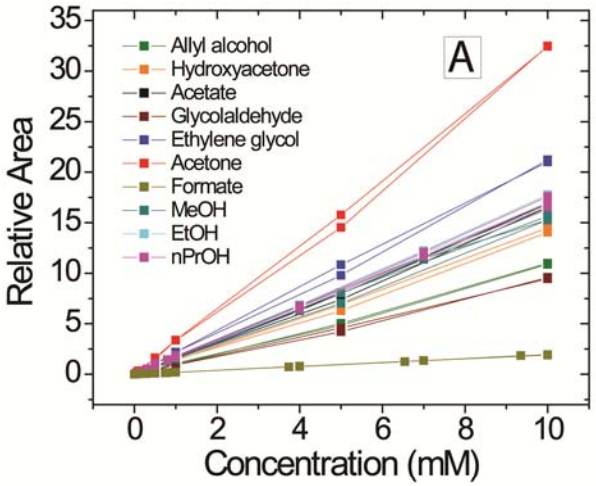

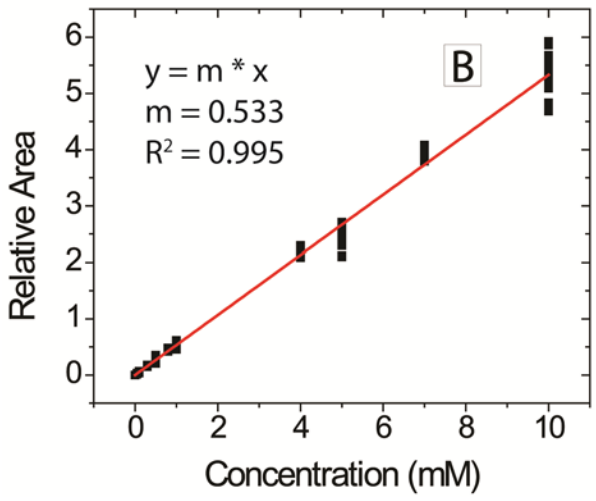

Figure S4. ^{1}H 1D NMR spectrum on a sample of 0.1 M KHCO3 containing a mixture of products. The spectrum was acquired on a 600 MHz Varian Inova with a 0.5 s prescan delay, 5 s presaturation of the H_2O resonance, 45 degree read-pulse, over an 8000 Hz spectral width, 4 s acquisition time, centered on the water peak, for 52 scans. The change in the baseline near the middle of the spectrum corresponds to the location of the suppressed water peak. Peak assignments are given in Table S1.

Figure S5. A) Standard curves for products constructed with authentic standards. B) Points of the top standard curves normalized to the number of protons represented by each peak and showing the linear regression line for the normalized points used to determine the concentration of acetaldehyde and propionaldehyde.

CO_2 Reduction Products							Assignment		Known Standards			
Chemical Shift	^{1}H splitting	J coupling	COSY cross peaks	^{13}C (HSQC)	^{13}C (1D)	^{13}C splitting	Probed Nucleus	Product Name	^{1}H splitting	Chemical Shift	J coupling	^{13}C (1D)
9.57	s						$CH_3CH_2C\,H{=}O$	Propionaldehyde	s	9.57		209.6
9.55	q	2.93	2.12				$CH_3C\,H{=}O$	Acetaldehyde	q	9.55	2.93	206.9
8.33	s			172.2	171.76	s	$HCOO^-$	Formate	s	8.33		171.77
					161.16		Bicarbonate	Electrolyte				162.97
					130.74		Phenol	Internal Standard	t	7.2	7.61	130.7
					121.24		Phenol	Internal Standard	t	6.86	7.61	121.07
					115.92		Phenol	Internal Standard	d	6.8	8.78	116.31
5.89	m		5.16, 5.06, 3.99	137.4	137.79	dd	$CH_2C\,HCH_2OH$	Allyl Alcohol	m	5.9		136.86
5.16	d	17.57	5.89, 3.99		116.36	d	CH_2CHCH_2OH	Allyl Alcohol	d	5.17	17.33	115.74
5.13	q	4.68	1.21		88.67	d	$CH_3C\,H(OH)_2$	Acetaldehyde	q	5.13	5.37	88.57
5.06	d	10.54	5.89, 3.99		116.36	d	CH_2CHCH_2OH	Allyl Alcohol	d	5.07	10.5	115.74
4.94	t	5.27	3.4		90.6	d	$(OH)_2C\,HCH_2OH$	Glycolaldehyde	t	4.94	5.13	90.63
4.843	t	5.27					$CH_3CH_2C\,H(OH)_2$	Propionaldehyde	t	4.85	5.87	92.77
					91.4	s	$(OH)_2\,CHCH(OH)_2$	Glyoxal				91.39
							WATER					
4.25	s						$CH_3C(=O)C\,H_2OH$	Hydroxyacetone	s	4.25		68.36
3.99	d	4.68	5.9, 5.15, 5.05	63.5	63.44	d	$CH_2C\,HCH_2OH$	Allyl Alcohol	dt	3.99	5.13, 1.46	62.96
3.545	s			63.65	63.41	s	$HOCH_2C\,H_2OH$	Ethylene Glycol	s	3.54		63.41
3.54	q	7.03	1.06	58.3	58.3	d	$CH_3C\,H_2OH$	Ethanol	q	3.53	7.32	58.3
3.44	t	7.03	1.42	64.35	64.42	d	$CH_2C\,H_2C\,H_2OH$	n-Propanol	t	3.44	6.49	64.43
3.4	d	4.68	4.94	65.6	65.38	d	$(OH)_2\,CHCH_2OH$	Glycolaldehyde	d	3.4	5.13	65.42
3.23	s			49.85	49.76	s	CH_3OH	Methanol	s	3.23		49.75
							DMSO	Internal Standard	s	2.6		39.6
2.44	q	7.03		37.25			$CH_3C\,H_2CH{=}O$	Propionaldehyde	q	2.44	7.32	37.34
2.12	d	2.93	9.55	30.94	30.8	d	$CH_3CH{=}O$	Acetaldehyde	d	2.12	2.93	30.89
2.1	s			30.9			$CH_3C{=}OC\,H_3$	Acetone	s	2.1		30.44
2.02	s			25.3			$CH_3C(=O)CH_2OH$	Hydroxyacetone	s	2.02		25.63
1.79	s			24	24.19	d	$CH_3C(=O)O^-$	Acetate	s	1.87		23.74
1.48	dt	5.85		30.95			$CH_3C\,H_2CH(OH)_2$	Propionaldehyde	dt	1.47	7.57, 12.94	30.45
1.42	sextet	6.44	3.44, 0.77	25.28	25.37	t	$CH_3C\,H_2CH_2OH$	n-Propanol	sextet	1.42	7.32	25.41
1.21	d	5.27	5.13	24	23.82	d	$CH_3CH(OH)_2$	Acetaldehyde	d	1.2	5.37	23.5
1.06	t	7.03	3.54	17.4	17.62	d	CH_3CH_2OH	Ethanol	t	1.06	7.08	17.63
0.92	t	7.61		5.74			$CH_3CH_2CH{=}O$	Propionaldehyde	t	0.92	7.32	5.54
0.78	t	7.61					$CH_3CH_2CH(OH)_2$	Propionaldehyde	t	0.78	7.32	8.47
0.77	t	7.61	1.42	10.2	10.34	d	$CH_3CH_2CH_2OH$	n-Propanol	t	0.77	7.57	10.36

Table S1. Product identification based on peak information for CO_2 reduction products compared to peak information for commercial authentic standards. Lines highlighted in blue indicate internal standard peaks and lines highlighted in green indicated CO_2 reduction product peaks used for quantification. Lines left white indicate peaks used to confirm the identity of the species, but were not used for quantification.

Relevant current density for solar fuels synthesis:

In the area of solar fuels, the energy of solar radiation is utilized to drive redox reactions for the synthesis of fuels. For example:

$2H^+ + 2e^- \rightarrow H_2$ (E_0 = 0.00 V/RHE), or $CO_2 + 6H^+ + 6e^- \rightarrow CH_3OH + H_2O$ (E_0 = +0.05 V/RHE)

For large scale solar fuel synthesis, water oxidation is the ideal source of the protons and electrons needed for the fuel-synthesis (reduction) reactions above, as water is inexpensive and abundant.[6,7]

$2H_2O \rightarrow 2O_2 + 4H^+ + 4e^-$ (E_0 = +1.23 V/RHE)

A current density of -10 $mA \cdot cm^{-2}$ for solar fuels synthesis is relevant because this current density roughly matches the spectrum for a 10% efficient solar-to-fuels device. Here, we show how we arrived at this value:

1. In a collaborative effort, the photovoltaics (PV) industry, government laboratories, and the American Society for Testing and Materials (ASTM) defined the standard terrestrial solar spectrum: AM1.5G.[8] Integration of this spectrum yields a value of 1000 $W \cdot m^{-2}$ = 100 $mW \cdot cm^{-2}$, an illumination intensity which is typically referred to as "1 sun".
2. Note that the red-ox potentials above for fuel synthesis and water oxidation are approximately 1.2 V apart. If 1 sun = 100 $mW \cdot cm^{-2}$ = 100 $(mA \cdot V) \cdot cm^{-2}$, then a 100 % efficient solar-to-fuel device would draw (100 $(mA \cdot V) \cdot cm^{-2}$)/(1.2 V) = 83 $mA \cdot cm^{-2}$ under AM1.5G.
3. A 10 % efficient solar-to-fuel device would draw 1/10th the current, at 8.3 $mA \cdot cm^{-2}$.

Determination of Error in Measurements

Multiple measurements were made at each potential to ascertain the repeatability of the experimental method and to reduce the effect of differences in factors such as the surface preparation between experiments. Although there is variation between experiments (Table S2), it is not unreasonably large. Figure S6 shows the current efficiency for different products plotted with error bars corresponding to one standard deviation. The error in current efficiency is largest when small quantities are measured, such as points taken at low overpotential or for minor products, due to errors in product detection. Error in current efficiency is also larger at high overpotential, which can be attributed to the rise in the uncertainty of the potential due to errors in the voltage due to IR compensation.

Average Values

Applied V vs Ag/AgCl	V vs RHE 100% IR	Current Efficiencies (fraction of total current): Formate	Allyl Alcohol	Ethylene Glycol	n-Propanol	Glycolaldehyde	Methanol	Acetone	Hydroxyacetone	Acetate	Acetaldehyde	Ethanol	Propionaldehyde	Hydrogen	Methane	CO	Ethylene
-1.95	-1.17	0.0046	0	0.0001	0.0013	0	0.0001	0	0	0.0004	0	0.0167	0	0.5574	0.4036	0.0029	0.0858
-1.875	-1.14	0.0081	0.0011	0.0008	0.0089	0.0062	0.0014	0.0004	0	0.0016	0.0017	0.0553	0.0000	0.3248	0.3990	0.0043	0.1532
-1.8	-1.09	0.0142	0.0087	0.0015	0.0208	0.0035	0.0004	0.0008	0	0.0023	0.0026	0.0920	0.0000	0.2220	0.2961	0.0063	0.2095
-1.725	-1.05	0.0205	0.0117	0.0013	0.0253	0.0028	0.0002	0.0008	0	0.0030	0.0034	0.0975	0.0000	0.2260	0.2441	0.0107	0.2598
-1.65	-1.01	0.1074	0.0162	0.0014	0.0401	0.0001	0.0003	0.0002	0.0004	0.0024	0.0017	0.0563	0.0048	0.2539	0.1743	0.0403	0.1793
-1.575	-0.96	0.1737	0.0024	0.0003	0.0268	0	0.0011	0.0001	0	0.0009	0.0014	0.0250	0.0045	0.3020	0.0302	0.0662	0.1021
-1.5	-0.89	0.2460	0	0	0	0	0	0	0	0	0	0	0	0.3766	0.0073	0.0874	0.0363
-1.425	-0.82	0.2270	0	0	0	0	0	0	0	0	0	0	0	0.4376	0.0014	0.0764	0.0184
-1.35	-0.75	0.1922	0	0	0	0	0	0	0	0	0	0	0	0.6181	0.0007	0.1147	0.0043
-1.275	-0.67	0.0859	0	0	0	0	0	0	0	0	0	0	0	0.7619	0	0.1837	0

Error Between Measurements

Number of Measurements	1 Standard Deviation: V	Formate	Allyl Alcohol	Ethylene Glycol	n-Propanol	Glycolaldehyde	Methanol	Acetone	Hydroxyacetone	Acetate	Acetaldehyde	Ethanol	Propionaldehyde	Hydrogen	Methane	CO	Ethylene
4	0.031	0.0031		0.0002	0.0018		0.0002			0.0002		0.0080		0.1679	0.1742	0.0024	0.0801
3	0.019	0.0010	0.0019	0.0001	0.0010	0.0079	0.0017	0.0002		0.0001	0.0008	0.0040		0.0536	0.0353	0.0007	0.0311
3	0.018	0.0006	0.0041	0.0004	0.0040	0.0013	0.0001	0.0002		0.0006	0.0006	0.0082		0.0157	0.0214	0.0019	0.0226
3	0.008	0.0024	0.0028	0.0001	0.0039	0.0011	0.0002	0.0002		0.0005	0.0022	0.0040		0.0096	0.0189	0.0016	0.0083
3	0.004	0.0572	0.0102	0.0015	0.0125	0.0002	0.0005	0.0003	0.0007	0.0025	0.0030	0.0088	0.0083	0.0046	0.0556	0.0188	0.0412
3	0.004	0.0987	0.0042	0.0005	0.0168		0.0019	0.0002		0.0011	0.0024	0.0160	0.0078	0.0675	0.0048	0.0117	0.0887
5	0.003	0.0731												0.0449	0.0035	0.0161	0.0205
3	0.003	0.0132												0.0215	0.0021	0.0157	0.0176
3	0.001	0.0677												0.1658	0.0012	0.0322	0.0051
3	0.001	0.0051												0.1779		0.1951	

Table S2. Average current efficiency data for experiments run at different potentials and the error between measurements at the same potential given as one standard deviation.

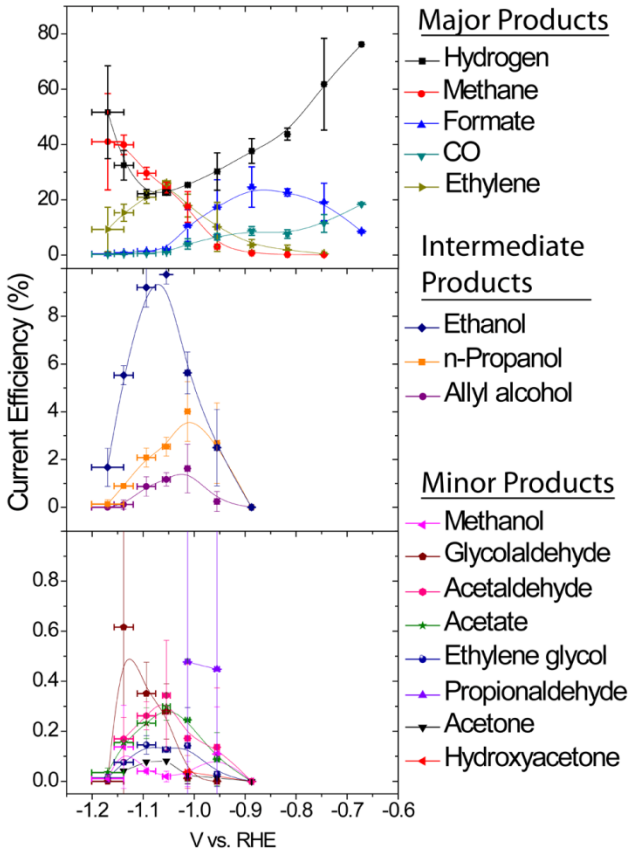

Figure S6. Current efficiency plot showing error bars of one standard deviation for the voltage and current efficiency at each point.

TOF

The TOF is shown in terms of umol·s^{-1}·cm^{-2} and molecules ·s^{-1}·surface Cu $atom^{-1}$ in Figure S7. The number of surface Cu atoms was used because we do not know the nature of the site that produces each of products. The number of surface atoms was estimated by assuming the atomic density of a Cu111 surface with a roughness factor of 2, which results in 3.8 x 10^{15} atoms·cm^{-2}. The calculated TOF is likely no more than a factor of 2 different from the true value.

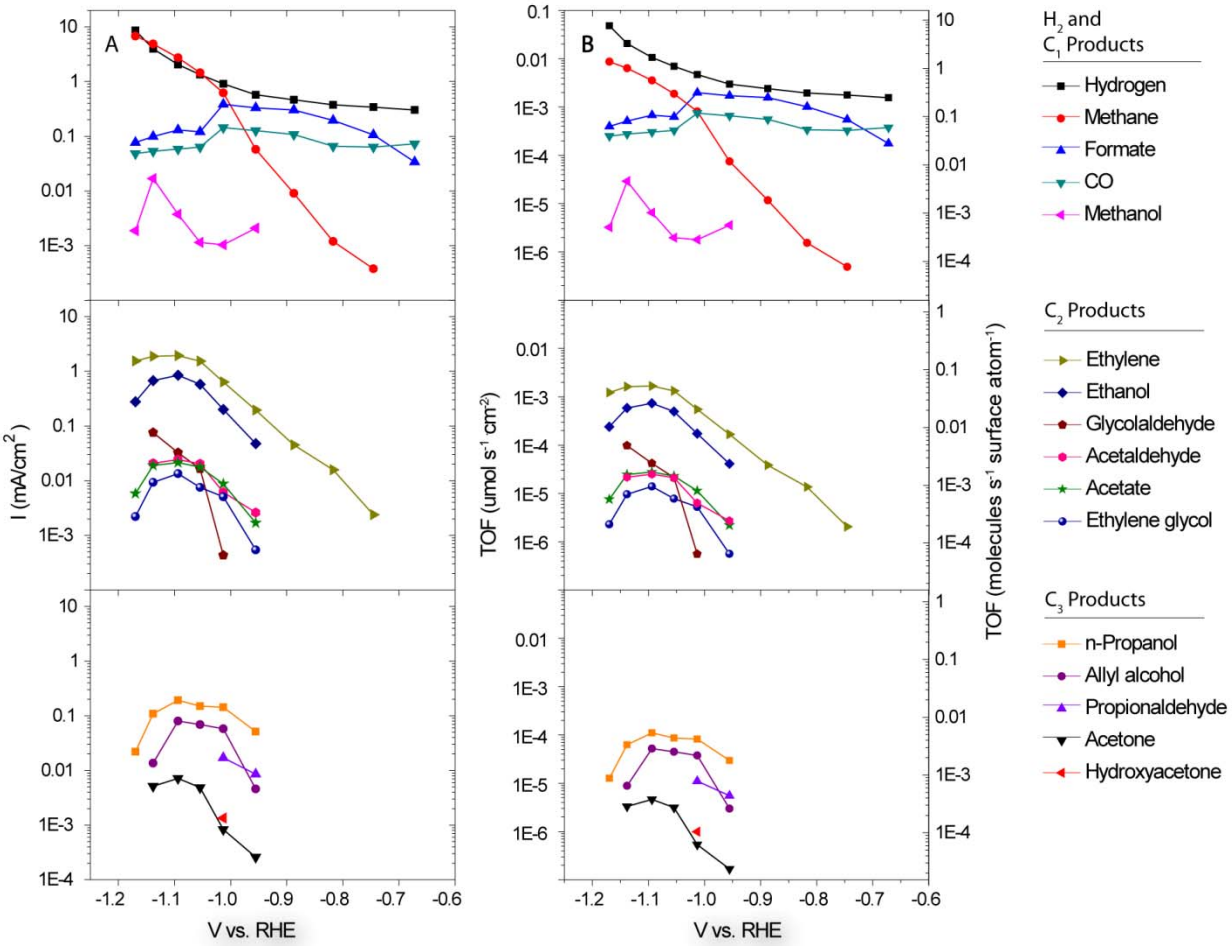

Figure S7. Tafel plot of (A) the partial current going to each product compared to (B) the corresponding TOF in terms of the geometric surface area.

References

(1) Myland, J. C.; Oldham, K. B. *Analytical Chemistry* **2000**, *72*, 3972.

(2) Allen J. Bard, L. R. F. *Electrochemical Methods: Fundamentals and Applications, Techniques Based on Concepts of Impedance*; John Wiley & Sons: New York, 1980.

(3) Allen J. Bard, L. R. F. *Electrochemical Methods: Fundamentals and Applications, Electronic Compensation of Resistance*; John Wiley & Sons: New York, 1980.

(4) van der Vliet, D.; Strmcnik, D. S.; Wang, C.; Stamenkovic, V. R.; Markovic, N. M.; Koper, M. T. M. *Journal of Electroanalytical Chemistry* **2010**, *647*, 29.

(5) Claridge, T. D. W. In *High-Resolution NMR Techniques in Organic Chemistry*; Elsevier: Oxford, 2006, p 114.

(6) Kanan, M. W.; Nocera, D. G. *Science* **2008**, *321*, 1072.

(7) Lewis, N. S.; Nocera, D. G. *Proc. Natl. Acad. Sci. U. S. A.* **2006**, *103*, 15729.

(8) http://rredc.nrel.gov/solar/spectra/am1.5/. [Online Early Access].